INORGANIC CHEMISTRY FRONTIERS

RESEARCH ARTICLE

View Article Online
View Journal | View Issue

Cite this: *Inorg. Chem. Front.*, 2023, **10**, 4425

A unique $[Sb_6O_2S_{13}]^{12-}$ finite chain in oxychalcogenide $Ba_6Sb_6O_2S_{13}$ leading to ultra-low thermal conductivity and giant birefringence†

Yong-Fang Shi,[a,b] Sheng-Hua Zhou,[a,b,c] Peng-Fei Liu,[d] Xin-Tao Wu,[a,b] Hua Lin *[a,b] and Qi-Long Zhu *[a,b]

Received 8th May 2023,
Accepted 20th June 2023

DOI: 10.1039/d3qi00850a

rsc.li/frontiers-inorganic

Recently, heteroanionic materials have been drawing wide attention due to their unique crystal structures which result in fascinating physical properties. However, reports on structural exploration and functional application of lone-pair-cation-based oxychalcogenides are still very rare. In this work, a new Sb-based oxysulfide, $Ba_6Sb_6O_2S_{13}$, was successfully obtained *via* a high-temperature solid-phase method. $Ba_6Sb_6O_2S_{13}$ belongs to the monoclinic space group of $P2_1/c$ (no. 14) and is formed by charge-balanced Ba^{2+} cations and zero-dimensional (0D) $[Sb_6O_2S_{13}]^{12-}$ finite chains made of the triangular-pyramid $[SbOS_2]$, quadrangular-pyramid $[SbOS_3]$ and teeter-totter $[SbS_4]$ units by sharing vertices. Note that the coexistence of various Sb-coordinated fashions in one material is surprisingly found for the first time. More encouragingly, such a unique 0D structure in $Ba_6Sb_6O_2S_{13}$ leads to an ultra-low thermal conductivity of 0.25 W m^{-1} K^{-1} at 700 K (one of the lowest values seen in a crystalline material) and a giant birefringence of 0.66 at 2050 nm (the highest value among metal chalcogenides reported thus far), which is further confirmed using theoretical calculations. As a result, this work will inspire intriguing and further research on heteroanionic materials with low-dimensional structures and hold great potential for their utilization in the photothermal field.

Introduction

In recent years, low-dimensional inorganic chalcogenides with unique chemical bonding characteristics (ionic, covalent, or van der Waals) have attracted great attention because of their intriguing physical properties, such as photocatalysis, photoluminescence, magnetism, superconductivity, thermoelectricity, and second-order nonlinear optics (NLO).[1] For example, a remarkable photocurrent response was observed in the pentanary chalcogenide $Rb_2Ba_3Cu_2Sb_2S_{10}$, in which the structure is formed by one-dimensional (1D) $[Cu_2Sb_2S_{10}]^{8-}$ chains.[2] The quaternary sulphide $Ba_8Zn_4Ga_2S_{15}$ possesses a 1D $[Zn_4Ga_2S_{15}]^{16-}$ chain structure and exhibits strong yellow photoluminescence emission at 298 K.[3] An unprecedented two-dimensional (2D) layered chalcohalide $Cs_2[Mn_2Ga_3S_7Cl]$ displays distinguishing structural features with the coexistence of two Mn-based coordination geometries and exhibits an impressive ferrimagnetic phenomenon below 16 K.[4] Two typical examples are the discovery of superconductivity in the ternary Bi-based tellurides $CsBi_4Te_6$ and $RbBi_{11/3}Te_6$, whose structures are made of alternately stacked 2D ionic $[Bi_4Te_6]^-$ and $[Bi_{11/3}Te_6]^-$ layers, respectively.[5] Single-crystal SnSe exhibits a high figure of merit (ZT of 2.3 ± 0.3 at 973 K along the c axis) with an extremely low intrinsic thermal conductivity (0.23 ± 0.03 W m^{-1} K^{-1} at 973 K) owing to the unique wrinkled 2D layered structure.[6] More recently, a quaternary non-centrosymmetric (NCS) material $SrCdSiS_4$, which features a 2D $[CdSiS_4]^{2-}$ layered structure, was reported to exhibit superior IR-NLO comprehensive performances.[7]

In contrast to extensively reported layered 2D and 1D chain chalcogenides, reports on zero-dimensional (0D), *e.g.* "molecular", inorganic chalcogenides are very scarce. On one hand, these 0D inorganic chalcogenides are mainly obtained through high-temperature solid-state methods. On the other hand, they have a simple structural composition and show a unique physical performance. For instance, the quaternary selenide

[a]*State Key Laboratory of Structural Chemistry, Fujian Institute of Research on the Structure of Matter, Chinese Academy of Sciences, Fuzhou 350002, China. E-mail: linhua@fjirsm.ac.cn, qlzhu@fjirsm.ac.cn*
[b]*Fujian Science & Technology Innovation Laboratory for Optoelectronic Information of China, Fuzhou 350002, China*
[c]*University of Chinese Academy of Sciences, Beijing 100049, China*
[d]*Spallation Neutron Source Science Center, Institute of High Energy Physics, Chinese Academy of Sciences, Dongguan 523803, China*

†Electronic supplementary information (ESI) available: Additional experimental and theoretical results, together with additional tables and figures. CCDC 2247687. For ESI and crystallographic data in CIF or other electronic format see DOI: https://doi.org/10.1039/d3qi00850a

$Ba_2AsGaSe_5$ shows a strong visible-light-induced photocatalytic performance (6.5 times larger than that of titanium dioxide powder (P25)), which can be attributed to the discrete novel $[AsGaSe_5]^{4-}$ clusters.[8] Strong second-harmonic generation (SHG) intensities were observed in the NCS chalcogenides $Ba_{23}Ga_8Sb_2S_{38}$ and $M_2As_2Q_5$ (M = Ba, Pb; Q = S, Se), in which the structure is composed of isolated $[GaS_4]$ tetrahedra and $[SbS_3]$ pyramids in the former and multiple discrete $[As_xQ_y]$ anions in the latter.[9] In the quaternary sulphide $Ba_3HgGa_2S_7$, the combination of seesaw-like $[HgS_2]$ units and tetrahedral $[GaS_4]$ groups prompts the formation of $[Hg_2Ga_4S_{14}]^{12-}$ strings which could increase the polarizability of the crystal structure, thus a large birefringence (0.09@2100 nm) was achieved in this compound.[10]

Oxychalcogenides, which combine two different types of anions in one structure (*i.e.*, high electronegativity O^{2-} and low electronegativity Q^{2-}), have emerged as a new type of low-dimensional functional material in recent years.[11] Despite a great number of reports on novel oxychalcogenides with 1D and 2D structures so far, the exploration of 0D structures, especially for Sb-based oxychalcogenides, is quite limited. Hence, in this work, we take interest in the AE/Sb/O/Q (AE = alkaline-earth metal elements; Q = S, Se) system, hoping to obtain low-dimensional structures. Fortunately, a novel Sb-based oxychalcogenide $Ba_6Sb_6O_2S_{13}$ with a 0D structure was discovered in this quaternary family. Notably, the $[Sb_6O_2S_{13}]^{12-}$ finite chain which is not normally found in inorganic chalcogenides is formed in this structure. Here, we report the solid-state synthesis, crystal structure, thermal transport and optical properties, as well as theoretical calculations of $Ba_6Sb_6O_2S_{13}$.

Table 1 Crystallographic information and refinement results for $Ba_6Sb_6O_2S_{13}$

Empirical formula	$Ba_6Sb_6O_2S_{13}$
CCDC number	2247687
Formula weight	2003.32
Temperature (K)	293(2)
Crystal size (mm)	0.15 × 0.10 × 0.10
Crystal system	Monoclinic
Space group	$P2_1/c$ (no. 14)
a (Å)	8.7497(7)
b (Å)	14.2018(8)
c (Å)	11.7822(8)
α (°)	90
β (°)	96.616(5)
γ (°)	90
V (Å^3)	1454.3(2)
Z	2
D_c (g cm^{-3})	4.575
μ (mm^{-1})	14.385
GOOF on F^2	1.052
R_1, wR_2 ($I > 2\sigma(I)$)[a]	0.0248, 0.0521
R_1, wR_2 (all data)	0.0271, 0.0534
Largest diff. peak and hole (e Å^{-3})	1.23, −2.03

[a] $R_1 = \sum||F_o| - |F_c||/\sum|F_o|$, $wR_2 = [\sum w(F_o^2 - F_c^2)^2/\sum w(F_o^2)^2]^{1/2}$.

Results and discussion

$Ba_6Sb_6O_2S_{13}$ represents a new combination of the quaternary AE/Sb/O/Q (AE = alkaline-earth metals; Q = chalcogen) system and belongs to the monoclinic space group of $P2_1/c$ (no. 14) [Pearson symbol: $mP54$; idealized Wyckoff sequence: $e^{13}a$] (Table 1). Its asymmetric unit is made up of 6 Ba, 6 Sb, 2 O and 13 S atoms, which are all at the Wyckoff position of 4*e* except O1 and O2 at 2*a* (Table 2). As illustrated in Fig. 1a, the Sb1 atom is coordinated to the 1 O atom and 2 S atoms forming a trigonal planar $[Sb1OS_2]$ basic building unit (BBU) while Sb3 atoms are surrounded by the 1 O atom and 3 S atoms in a distorted teeter-totter $[Sb2OS_3]$ environment. The Sb2 atom shows a common teeter-totter coordination mode with 4 S atoms. It is worth mentioning that the coordination diversity of Sb atoms (*i.e.*, $[SbOS_2]$, $[SbOS_3]$, and $[SbS_4]$) in a single structure has been discovered for the first time. The Sb–O and Sb–S distances are 2.023–2.085 and 2.393–2.858 Å (Table S1†), respectively, which are comparable to those in the reported Sb-based chalcogenides.[12] The heteroanionic $[Sb1OS_2]$ and $[Sb3OS_3]$ BBUs adopt O-sharing and S4-sharing to form $[Sb_2S_4O]^{4-}$ groups, which are further connected by isolated $[SbS_4]$ units resulting in a unique finite $[Sb_6O_2S_{13}]^{12-}$

Table 2 The atomic coordinates and equivalent isotropic displacement parameters for $Ba_6Sb_6O_2S_{13}$

Atom	Wyckff.	x	y	z	U_{eq}/Å^2	BVS
Ba1	4*e*	0.29892(4)	0.13605(3)	0.09160(3)	0.00175(2)	1.96
Ba2	4*e*	0.59957(4)	0.16259(3)	0.45656(3)	0.00153(2)	1.85
Ba3	4*e*	0.90869(4)	0.36339(3)	0.28593(3)	0.00165(2)	1.96
Sb1	4*e*	0.15729(5)	0.39552(3)	0.96110(4)	0.00142(2)	2.87
Sb2	4*e*	0.80265(5)	0.11340(3)	0.11129(4)	0.00227(2)	3.25
Sb3	4*e*	0.39253(6)	0.38288(4)	0.22091(4)	0.00293(2)	2.85
O	4*e*	0.3381(5)	0.3300(3)	0.0620(4)	0.00150(9)	2.01
S1	4*e*	1	0	0	0.00365(7)	1.91
S2	4*e*	0.3268(2)	0.4891(2)	0.8539(2)	0.00163(3)	1.68
S3	4*e*	0.2440(2)	0.2778(2)	0.3231(2)	0.00181(4)	1.93
S4	4*e*	0.1412(2)	0.4986(2)	0.1287(2)	0.00217(4)	1.64
S5	4*e*	0.9404(2)	0.2469(2)	0.0440(2)	0.00179(3)	1.91
S6	4*e*	0.6129(2)	0.2376(2)	0.2100(2)	0.00267(4)	2.05
S7	4*e*	0.6150(2)	0.0967(2)	0.9479(2)	0.00200(4)	1.91

U_{eq} is defined as one third of the trace of the orthogonalized U_{ij} tensor.

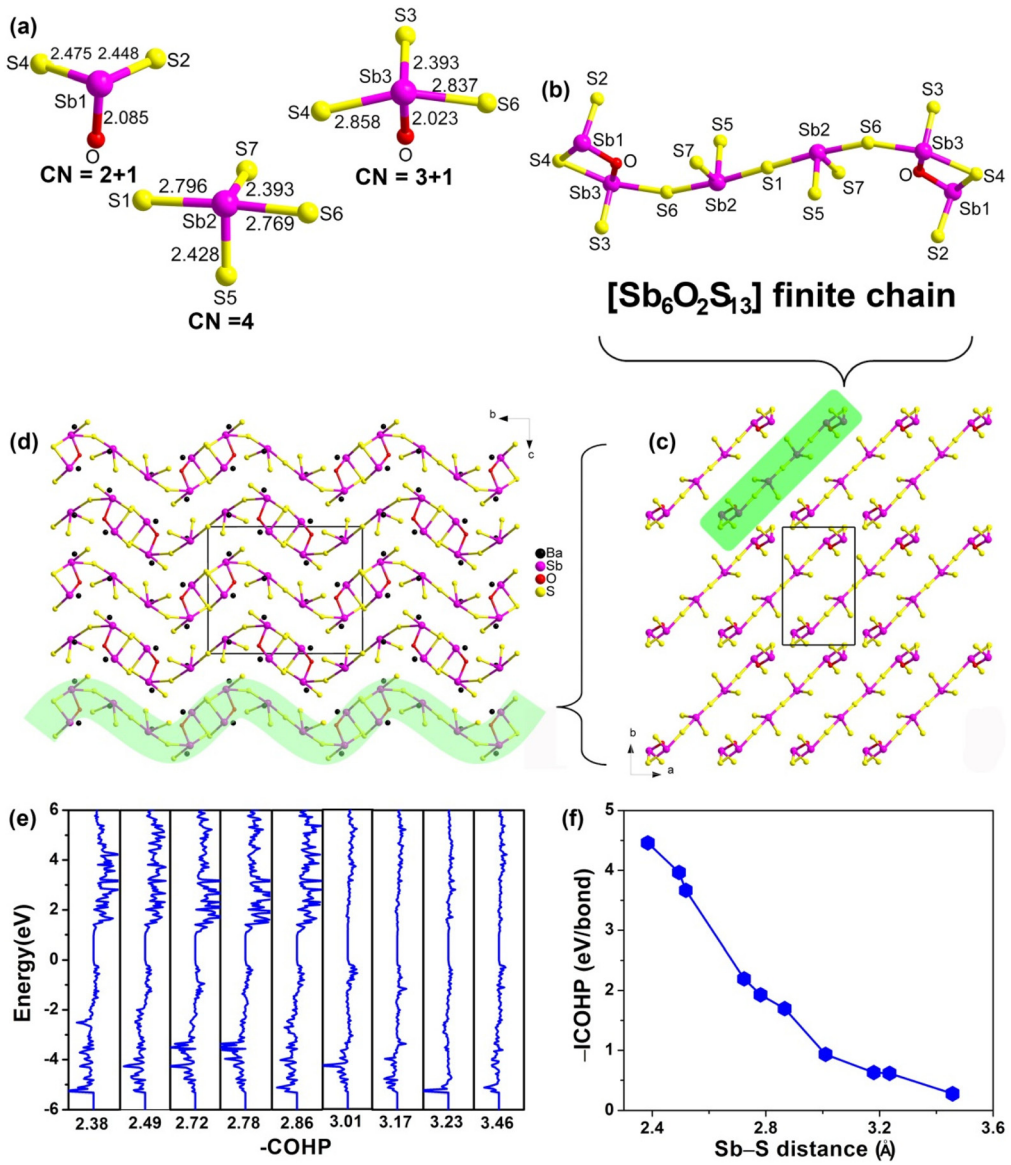

Fig. 1 (a) Coordination modes of $[SbOS_2]$, $[SbOS_3]$ and $[SbS_4]$ BBUs; (b) coordination environment of the $[Sb_6O_2S_{13}]^{12-}$ finite chain with marked atom numbers; (c) distribution of 0D finite chains on the *ab* plane; (d) ball-and-stick representation of the unique 0D finite chain structure of $Ba_6Sb_6O_2S_{13}$ viewed along the *bc* plane; (e) the COHP diagram for Sb–S bond distances; (f) ICOHP plotted against Sb–S bond distances.

chain (Fig. 1b). The specific distributions of these finite $[Sb_6O_2S_{13}]^{12-}$ chains parallel to the *a*–*b* plane and *b*–*c* plane are shown in Fig. 1c and d, respectively. The charge-balanced Ba^{2+} cations are distributed in the spaces of finite $[Sb_6O_2S_{13}]^{12-}$ chains, that possess two different coordination modes, *i.e.*, $[BaS_8]$ and $[BaOS_8]$ polyhedra, with Ba–S distances of 3.110–3.702 Å and Ba–O distances of 2.728–2.802 Å (Fig. S1 and Table S1†). The valence states of Ba, Sb, O, and S atoms are determined as 2+, 3+, 2−, and 2−, respectively, according to BVS calculations.[13] Actually, there still exist 4 other Sb–S interactions with bond distances of 3.01–3.46 Å, which are much larger than the average Sb–S bond distance (2.65 Å) in the structure of $Ba_6Sb_6O_2S_{13}$. For this reason, the detailed COHP and ICOHP were applied to the in-depth study of the interaction characteristics between Sb and S.[14] As plotted in Fig. 1e and d, the results of the crystal orbital Hamiltonian population (COHP) and integrated COHP (ICOHP) analyses indicate that the bonding interactions of the short Sb–S bonds (2.38–2.86 Å) are much stronger than those of the long Sb–S bonds (3.01–3.46 Å), which supports the coordination environment of Sb atoms in the above-mentioned structural analysis.

It is very interesting to compare the above structures with the previously reported structures of $Ba_2Sb_2O_2S_3$[15] and $Ba_2Sb_2O_5$.[16] From the perspective of structural chemistry, quaternary $Ba_6Sb_6O_2S_{13}$ and $Ba_2Sb_2O_2S_3$ (denoted as $Ba_6Sb_6O_6S_9$) oxychalcogenides can be considered as derivatives by the partial chemical substitution approach (*i.e.*, partial O is replaced by S atoms) with ternary $Ba_2Sb_2O_5$ (denoted as

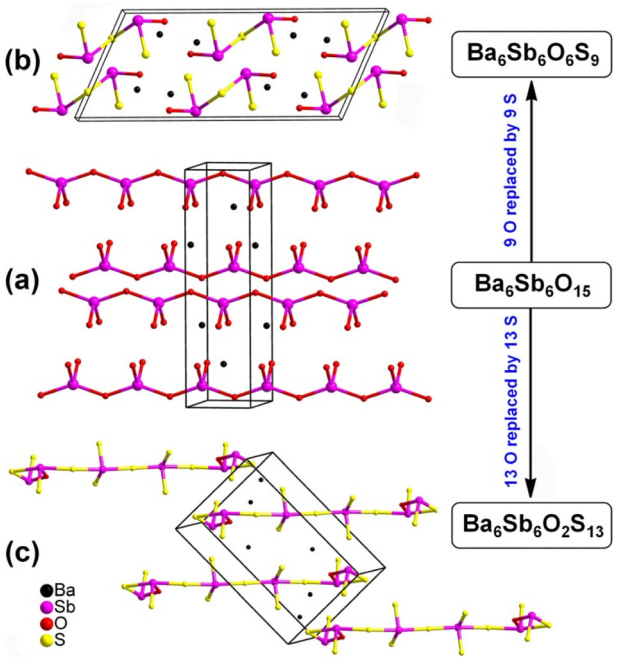

Fig. 2 Structural evolutions from (a) ternary $Ba_2Sb_2O_5$ (denoted as $Ba_6Sb_6O_{15}$) to quaternary oxychalcogenide (b) $Ba_2Sb_2O_2S_3$ (denoted as $Ba_6Sb_6O_6S_9$) and (c) $Ba_6Sb_6O_2S_{13}$ by the partial chemical substitution approach.

$Ba_6Sb_6O_{15}$) as the structural template (see Fig. 2 for details). They have a similar molecular formula, but they exhibit some significantly different structural features: (i) $Ba_2Sb_2O_5$ is crystalline in the orthorhombic crystal system, whereas $Ba_6Sb_6O_2S_{13}$ and $Ba_2Sb_2O_2S_3$ belong to the monoclinic crystal system; (ii) 1D infinite $[Sb_2O_5]^{4-}$ chains are isolated in $Ba_2Sb_2O_5$, whereas 0D finite $[Sb_6O_2S_{13}]^{12-}$ chains and isolated $[Sb_2O_2S_3]^{4-}$ clusters are found in $Ba_6Sb_6O_2S_{13}$ and $Ba_2Sb_2O_2S_3$, respectively; (iii) compounds $Ba_2Sb_2O_5$ and $Ba_2Sb_2O_2S_3$ possess only one type of Sb-based BBU, *i.e.*, $[SbO_4]$ and $[SbO_2S]$, while $Ba_6Sb_6O_2S_{13}$ shows three different kinds of BBUs, *i.e.*, $[SbOS_2]$, $[SbOS_3]$, and $[SbS_4]$. Fig. 2 clearly shows the detailed structural evolution from the $Ba_2Sb_2O_5$ prototype to the derived $Ba_2Sb_2O_2S_3$ and $Ba_6Sb_6O_2S_{13}$. In brief, these findings not only enrich the structural library of heteroanionic compounds but also provide a new approach for designing and exploring new low dimensional oxychalcogenides.

Furthermore, the properties of the title compound together with other previously reported Sb-based oxychalcogenides are briefly analysed, concluded and summarized (see Table S2† for details).[12b,15,17] From the perspective of structural chemistry, their composition can generally be divided into two parts: charge-balanced cations and anionic substructure. The former is mainly composed of alkaline-earth metals (*e.g.*, Ca, Sr, and Ba) as well as a small amount of rare earth elements (*e.g.*, La and Ce) and Pb, while the latter shows diversity in structural dimensions. Structural analysis shows that there are two main types of BBUs for Sb atoms with stereochemically-active-lone-pairs (SCALPs) in the anionic substructure, *i.e.*, monoanionic $[SbO_n]/[SbQ_n]$ (n = 3, 4, and 5) and heteroanionic $[SbO_xQ_y]$ ($x + y$ = 3, 4, and 5) BBUs. Then, these Sb-based BBUs are further connected to each other or other metal-based BBUs to generate 0D molecules, 1D chains, 2D layers, 3D networks or mixed-dimensional structures. As given in Table S2,† all these oxychalcogenides possess high S-to-O ratios and crystallize in low symmetry monoclinic space groups, except for orthorhombic $La_6Sb_4O_{12}S_3$. Moreover, most of them have a 2D layered structure (*ca.* 40%). Usually, low-dimensional chalcogenides can be obtained by enhancing the proportion of charge-balanced cations according to the viewpoint of "dimensional reduction".[18] Actually, this structural law is not followed in this quaternary family, for instance, $Ba_2Sb_2O_2S_3$, $Sr_2Sb_2O_2Se_3$, and $Sr_{3.5}Pb_{2.5}Sb_6O_5Se_{10}$, have the same [X/Sb] ratio of 1.0, but their corresponding structural dimensions are 0D, 1D, and 2D, respectively. Similar phenomena can also be observed in other SCALP-based chalcogenide systems.[19]

Single crystals of $Ba_6Sb_6O_2S_{13}$ were obtained by high temperature solid-state reactions of a mixture of BaS, Sb_2O_3 and Sb_2S_3 at 973 K (see the Experimental section in the ESI†). The elemental distributions of Ba : Sb : O : S were determined by EDX mapping as 6 : 6 : 2 : 13 (Fig. 3a and S2†), which are consistent with the results of single-crystal XRD analysis. The experimental powder XRD patterns matched with the simulated ones very well (Fig. 3b), without other impurities being present. UV–Vis–NIR diffuse reflectance spectroscopy was carried out to investigate the optical absorption properties of the title compound. As presented in Fig. 3c, the deduced optical E_g value of $Ba_6Sb_6O_2S_{13}$ is 1.68 eV, which is obviously smaller than that of the previously reported $Ba_2Sb_2O_2S_3$ (2.78 eV). Such significant change in the E_g value can be attributed to different O-to-S ratios, that is, the more O atoms are replaced by S atoms, the smaller E_g value is obtained. Moreover, TG and DSC measurements under a N_2 atmosphere indicate that $Ba_6Sb_6O_2S_{13}$ exhibits no obvious weight loss in the range of 300–1123 K. In addition, the DSC data show only one obvious endothermic peak at around 1017 K in the heating curve and one obvious exothermic peak at 953 K in the cooling curve, which illustrates $Ba_6Sb_6O_2S_{13}$ is a congruently melting compound (Fig. 3d).

In addition, inspired by a recent study that metal chalcogenides containing SCALPs exhibit extremely low intrinsic thermal conductivities,[20] we investigated the thermal transmission performance of $Ba_6Sb_6O_2S_{13}$. As shown in Fig. 4a, the total thermal conductivity (κ_T) of the polycrystalline $Ba_6Sb_6O_2S_{13}$ sample was measured in the temperature range of 303 to 723 K. It can be clearly seen that the κ_T value of $Ba_6Sb_6O_2S_{13}$ gradually decreases to an ultra-low value from ~0.38 W m^{-1} K^{-1} (at 303 K) to ~0.25 W m^{-1} K^{-1} (at 723 K) on heating the sample. As is known, the κ_T value is the summation of lattice thermal conductivity (κ_L) and electrical thermal conductivity (κ_E) values.[21] Since the E_g value of the title compound is large compared with that of classical thermoelectric materials, κ_E can be ignored, which means that the κ_T value of $Ba_6Sb_6O_2S_{13}$ can be considered as κ_L.[22] Moreover,

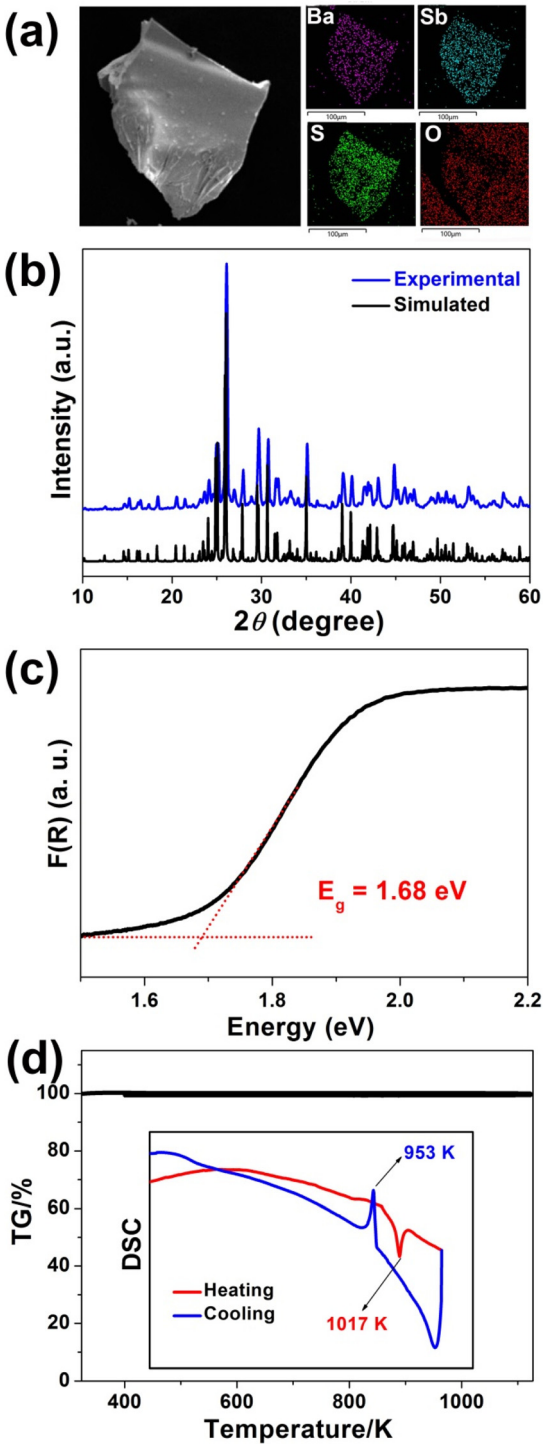

Fig. 3 Experimental characterization of $Ba_6Sb_6O_2S_{13}$: (a) the SEM image and the corresponding elemental mapping analysis; (b) experimental (blue) and simulated (black) PXRD patterns; (c) the solid-state diffuse-reflectance spectrum; (d) TG diagram (inset: DSC cyclic curves).

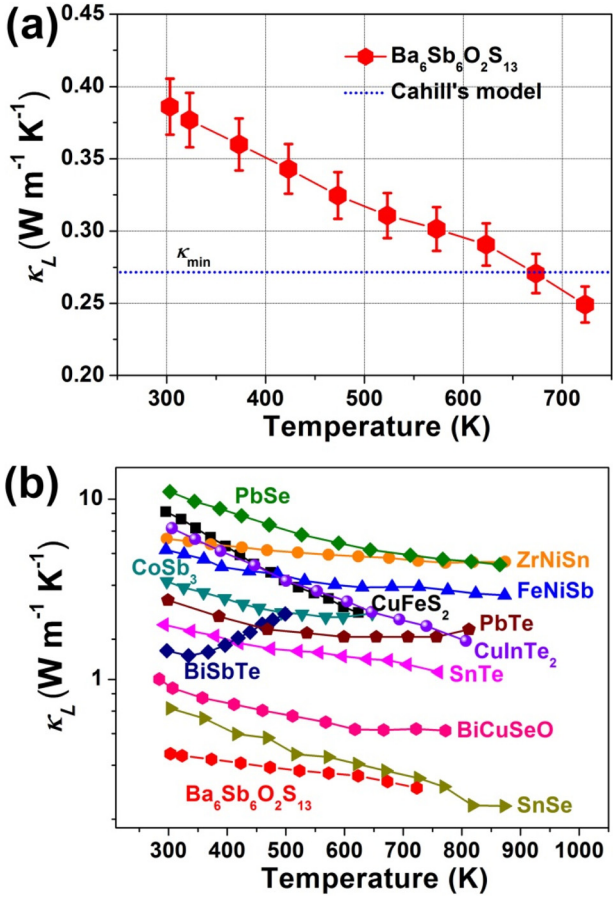

Fig. 4 (a) Lattice thermal conductivity (k_L) as a function of temperature for $Ba_6Sb_6O_2S_{13}$ (the dashed line represents the minimum k_L value calculated within the Cahill model) and (b) comparison of k_L with other reported state-of-the-art thermoelectric materials.

the calculated minimum lattice thermal conductivity (κ_{min}) of $Ba_6Sb_6O_2S_{13}$ was estimated using Cahill's model at about 0.27 W m^{-1} K^{-1}.[23] The reason for $Ba_6Sb_6O_2S_{13}$ possessing an ultra-low κ_L value can be mainly attributed to the following two aspects: (i) strongly ionic Ba^{2+} cations can decrease the phonon velocity and boost the phonon scattering ratio, and similar examples can also be found in other Ba-based systems;[24] (ii) due to the coexistence of multiple BBUs, the highly polarized [$SbOS_2$] triangular pyramid, [$SbOS_3$], and the [SbS_4] square pyramid can effectively enhance the lattice anharmonicity.[25] Therefore, the low κ_L value for $Ba_6Sb_6O_2S_{13}$ was verified through experimental measurement and theoretical estimation. Fig. 4b shows the temperature dependence of the κ_L value of $Ba_6Sb_6O_2S_{13}$ as well as those of some classical thermoelectric materials, including PbSe (~10.9–4.3 W m^{-1} K^{-1}),[26] $CuFeS_2$ (~8.5–2.3 W m^{-1} K^{-1}),[27] $CuInTe_2$ (~6.9–1.7 W m^{-1} K^{-1}),[28] ZrNiSn (~6.1–4.5 W m^{-1} K^{-1}),[29] FeNiSb (~5.2–3.0 W m^{-1} K^{-1}),[30] $CoSb_3$ (~3.6–2.3 W m^{-1} K^{-1}),[31] PbTe (~2.8–1.9 W m^{-1} K^{-1}),[32] SnTe (~2.0–1.1 W m^{-1} K^{-1}),[33] BiSbTe (~2.3–1.5 W m^{-1} K^{-1}),[34] BiCuSeO (~1.0–0.5 W m^{-1} K^{-1})[35] and SnSe (~0.7–0.2 W m^{-1} K^{-1})[36] for comparison.

To gain further insight into the relationship between the crystal structure and optical properties, theoretical investigations based on the density functional theory (DFT) were performed on $Ba_6Sb_6O_2S_{13}$. The electronic band structure along

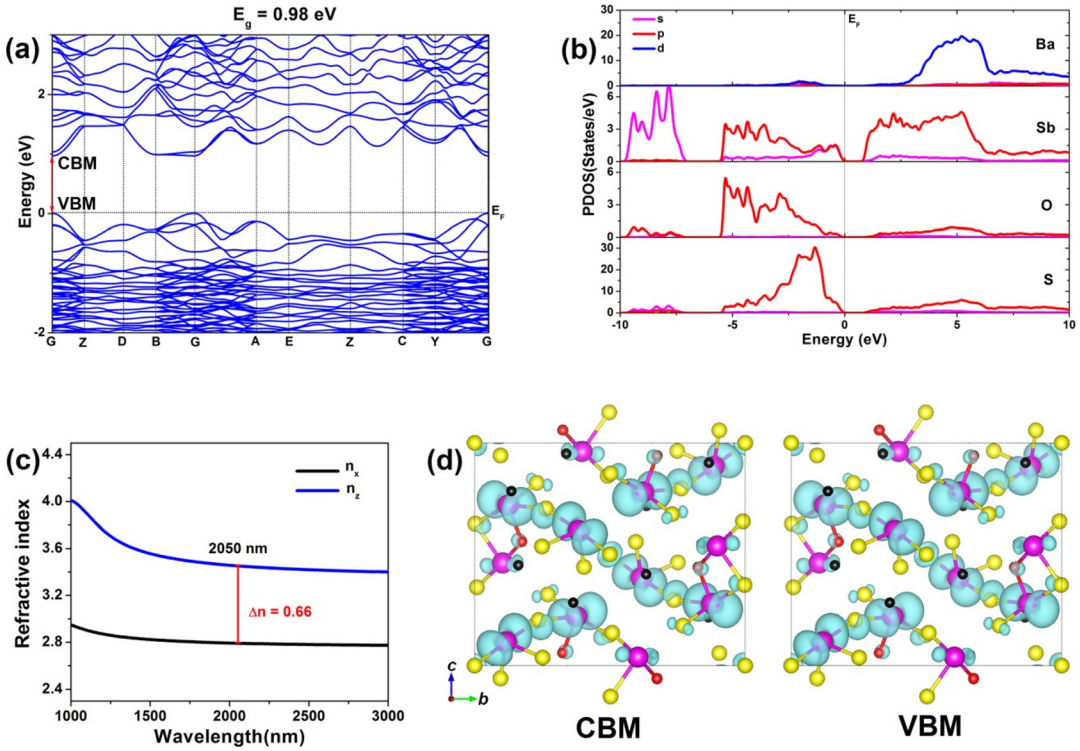

Fig. 5 Theoretical calculated results of $Ba_6Sb_6O_2S_{13}$: (a) calculated band structure; (b) PDOSs; (c) calculated birefringence (Δn); (d) projection of the charge density maps with major contributions in the CBM and VBM sections. Black atoms: Ba; pink atoms: Sb; red atoms: O; yellow atoms: S.

high symmetry points of the first Brillouin zone is plotted as shown in Fig. 5a and S3,† which reveals that $Ba_6Sb_6O_2S_{13}$ is a direct band-gap semiconductor with an E_g value of 0.98 eV at the G-point. Although this value is smaller than the experimentally obtained value of 1.68 eV, standard exchange–correlation functionals in DFT are well-known for underestimating E_g.[37] As shown by the partial density of states (PDOS) in Fig. 5b, O-2p S-3p and Sb-5s/5p states provide dominant contributions to the top of the valence band (VB), while the bottom of the conduction band (CB) of $Ba_6Sb_6O_2S_{13}$ is mainly constituted by S-3p and Sb-5p states, with little contributions from the O-2p and Ba-4d states. It can be concluded that the E_g of $Ba_6Sb_6O_2S_{13}$ is determined by $[SbOS_2]$, $[SbOS_3]$, and $[SbS_4]$ BBUs, that is, 0D finite $[Sb_6O_2S_{13}]^{12-}$ chains.

It is generally believed that a large anisotropy of low dimensional structures is beneficial for obtaining a larger Δn value.[38] Given that, also the refractive index was recorded and charge density maps were plotted to offer a more intuitive understanding of the structure–activity relationship. As displayed in Fig. 5c, $Ba_6Sb_6O_2S_{13}$ exhibits a huge Δn value throughout the entire calculation range. Among them, the calculated Δn value is 0.66@2050 nm, greater than those of recently reported low-dimensional chalcogenides with SCALPs, such as $RbBiP_2S_6$ ($\Delta n_{(cal.)}$ = 0.061@2050 nm),[39] $K_2Ag_3Sb_3S_7$ ($\Delta n_{(cal.)}$ = 0.165@2050 nm),[40] $Ba_2As_2Se_5$ ($\Delta n_{(cal.)}$ = 0.249@2050 nm),[9b] $CsZnAsSe_3$ ($\Delta n_{(cal.)}$ = 0.301@2050 nm),[41] and $CsCu_3SbS_4$ ($\Delta n_{(cal.)}$ = 0.442@2050 nm),[42] which indicates that $Ba_6Sb_6O_2S_{13}$ can be a promising IR birefringent candidate. Additionally, the experimental results also confirmed that the title compound has a wide IR transmission range from 0.75 to 18.3 μm (Fig. S4†). Furthermore, the calculation results based on the visual charge density maps (Fig. 5d) and electron localization function diagram (Fig. S5†) indicate that the synergistic effect of SCALP-based $[SbOS_2]$, $[SbOS_3]$, and $[SbS_4]$ BBUs in the 0D finite $[Sb_6O_2S_{13}]^{12-}$ chains of $Ba_6Sb_6O_2S_{13}$ is the core contribution for obtaining a giant Δn value.

Conclusions

In summary, a novel quaternary Sb-based oxychalcogenide, $Ba_6Sb_6O_2S_{13}$, has been successfully obtained by a conventional solid-state method at 973 K. The discrete $[Sb_6O_2S_{13}]^{12-}$ finite chain, formed by triangular-pyramid $[SbOS_2]$, quadrangular-pyramid $[SbOS_3]$ and teeter-totter $[SbS_4]$ units, is observed for the first time. UV-Vis-NIR spectroscopy measurement shows that $Ba_6Sb_6O_2S_{13}$ possesses an optical E_g value of 1.68 eV. Benefiting from the ordered arrangement of 0D $[Sb_6O_2S_{13}]^{12-}$ finite chains, the title compound exhibits an ultra-low thermal conductivity (0.25 W m^{-1} K^{-1} at 700 K) and an ultra-high birefringence (0.66 at 2050 nm). This work offers some new insights on Sb-based heteroanionic materials which would stimulate more exploratory syntheses and further enrich functional oxychalcogenides.

Author contributions

Y.-F. Shi prepared the samples, designed and carried out the experiments. S. H. Zhou and P. F. Liu carried out the theoretical calculations. X.-T. Wu provided discussion on the structure–property relationship of the title compound. H. Lin and Q.-L. Zhu conceived the experiments, analyzed the results and wrote and edited the manuscript. All the authors have approved the final version of the manuscript.

Conflicts of interest

There are no conflicts to declare.

Acknowledgements

This work was supported by the National Natural Science Foundation of China (22175175), the Fujian Science & Technology Innovation Laboratory for Optoelectronic Information of China (2021ZR118), and the Natural Science Foundation of Fujian Province (2022L3092).

References

1 (*a*) Y. Qi and A. M. Rappe, Widespread Negative Longitudinal Piezoelectric Responses in Ferroelectric Crystals with Layered Structures, *Phys. Rev. Lett.*, 2021, **126**, 217601; (*b*) J. D. Zhou, J. H. Lin, X. W. Huang, Y. Zhou, Y. Chen, J. Xia, H. Wang, Y. Xie, H. M. Yu and J. C. Lei, A library of atomically thin metal chalcogenides, *Nature*, 2018, **556**, 355–359; (*c*) A. P. Ramirez, R. J. Cava and J. Krajewski, Colossal magnetoresistance in Cr-based chalcogenide spinels, *Nature*, 2020, **386**, 156–159; (*d*) C. Chang, M. H. Wu, D. S. He, Y. L. Pei, C. F. Wu, X. F. Wu, H. L. Yu, F. Y. Zhu, K. D. Wang, Y. Chen, L. Huang, J. F. Li, J. Q. He and L. D. Zhao, 3D charge and 2D phonon transports leading to high out-of-plane ZT in n-type SnSe crystals, *Science*, 2018, **360**, 778–782; (*e*) M. Y. Li, Y. M. Shi, C. C. Cheng, L. S. Lu, Y. C. Lin, H. L. Tang, M. L. Tsai, C. W. Chu, K. H. Wei and J. H. He, Epitaxial growth of a monolayer WSe_2-MoS_2 lateral p-n junction with an atomically sharp interface, *Science*, 2015, **349**, 524–528; (*f*) H. Chen, W. B. Wei and H. Lin, Transition-metal-based Chalcogenides: A Rich Source of Infrared Nonlinear Optical Materials, *Coord. Chem. Rev.*, 2021, **448**, 214154; (*g*) H.-D. Yang, M.-Y. Ran, W.-B. Wei, X.-T. Wu, H. Lin and Q.-L. Zhu, Recent advances in IR nonlinear optical chalcogenides with well-balanced comprehensive performance, *Mater. Today Phys.*, 2023, **35**, 101127.

2 C. Liu, Y. Xiao, H. Wang, W. X. Chai, X. F. Liu, D. M. Yan, H. Lin and Y. Liu, One-Dimensional Chains in Pentanary Chalcogenides $A_2Ba_3Cu_2Sb_2S_{10}$ (A = K, Rb, Cs) Displaying a Photocurrent Response, *Inorg. Chem.*, 2020, **59**, 1577–1581.

3 Y. Y. Li, P. F. Liu, H. Lin, L. M. Wu, X. T. Wu and Q. L. Zhu, Quaternary semiconductor $Ba_8Zn_4Ga_2S_{15}$ featuring unique one-dimensional chains and exhibiting desirable yellow emission, *Chem. Commun.*, 2019, **55**, 7942–7945.

4 Y. J. Zheng, Y. F. Shi, C. B. Tian, H. Lin, L. M. Wu, X. T. Wu and Q. L. Zhu, An unprecedented pentanary chalcohalide with Mn atoms in two chemical environments: unique bonding characteristics and magnetic properties, *Chem. Commun.*, 2019, **55**, 79–82.

5 (*a*) C. D. Malliakas, D. Y. Chung, H. Claus and M. G. Kanatzidis, Superconductivity in the Narrow Gap Semiconductor $RbBi_{11/3}Te_6$, *J. Am. Chem. Soc.*, 2016, **138**, 14694–14698; (*b*) C. D. Malliakas, D. Y. Chung, H. Claus and M. G. Kanatzidis, Superconductivity in the Narrow Gap Semiconductor $CsBi_4Te_6$, *J. Am. Chem. Soc.*, 2013, **135**, 14540–14543.

6 L.-D. Zhao, G. Tan, S. Hao, J. He, Y. Pei, H. Chi, H. Wang, S. Gong, H. Xu, V. P. Dravid, G. J. Snyder, C. Wolverton and M. G. Kanatzidis, Ultrahigh power factor and thermoelectric performance in hole-doped single-crystal SnSe, *Science*, 2016, **351**, 141–144.

7 H. D. Yang, M. Y. Ran, S. H. Zhou, X. T. Wu, H. Lin and Q. L. Zhu, Rational design via dual-site aliovalent substitution leads to an outstanding IR nonlinear optical material with well-balanced comprehensive properties, *Chem. Sci.*, 2022, **13**, 10725–10733.

8 C. Li, X. S. Li, H. W. Huang, J. Y. Yao and Y. C. Wu, $Ba_2AsGaSe_5$: A New Quaternary Selenide with the Novel $[AsGaSe_5]^{4-}$ Cluster and Interesting Photocatalytic Properties, *Inorg. Chem.*, 2015, **54**, 9785–9789.

9 (*a*) M. C. Chen, L. M. Wu, H. Lin, L. J. Zhou and L. Chen, Disconnection Enhances the Second Harmonic Generation Response: Synthesis and Characterization of $Ba_{23}Ga_8Sb_2S_{38}$, *J. Am. Chem. Soc.*, 2012, **134**, 6058–6060; (*b*) M. M. Chen, Z. J. Ma, B. X. Li, W. B. Wei, X. T. Wu, H. Lin and Q. L. Zhu, $M_2As_2Q_5$ (M = Ba, Pb; Q = S, Se): a source of infrared nonlinear optical materials with excellent overall performance activated by multiple discrete arsenate anions, *J. Mater. Chem. C*, 2021, **9**, 1156–1163.

10 X. Huang, S. H. Yang, W. L. Liu and S. P. Guo, $Ba_3HgGa_2S_7$: A Zero-Dimensional Quaternary Sulfide Featuring a Unique $[Hg_2Ga_4S_{14}]^{12-}$ String and Exhibiting a High Photocurrent Response, *Inorg. Chem.*, 2022, **61**, 12954–12958.

11 (*a*) M. Y. Ran, Z. J. Ma, H. Chen, B. X. Li, X. T. Wu, H. Lin and Q. L. Zhu, Partial Isovalent Anion Substitution to Access Remarkable Second-Harmonic Generation Response: A Generic and Effective Strategy for Design of Infrared Nonlinear Optical Materials, *Chem. Mater.*, 2020, **32**, 5890–5896; (*b*) Y. F. Shi, W. B. Wei, X. T. Wu, H. Lin and Q. L. Zhu, Recent progress in oxychalcogenides as IR nonlinear optical materials, *Dalton Trans.*, 2021, **50**, 4112–4118; (*c*) Y. Zhang, H. Wu, Z. Hu and H. Yu, Oxychalcogenides: A Promising Materials Class for Nonlinear Optical Crystals with Mixed-anion Groups, *Chem. – Eur. J.*, 2022, **28**, e202203597; (*d*) M.-Y. Ran, S.-H. Zhou, B. Li, W. Wei, X.-T. Wu, H. Lin and Q.-L. Zhu, Enhanced Second-

Harmonic-Generation Efficiency and Birefringence in Melilite Oxychalcogenides $Sr_2MGe_2OS_6$ (M = Mn, Zn, and Cd), *Chem. Mater.*, 2022, **34**, 3853–3861; (*e*) R. Wang, F. Liang, X. Liu, Y. Xiao, Q. Liu, X. Zhang, L. M. Wu, L. Chen and F. Huang, Heteroanionic Melilite Oxysulfide: A Promising Infrared Nonlinear Optical Candidate with a Strong Second-Harmonic Generation Response, Sufficient Birefringence, and Wide Bandgap, *ACS Appl. Mater. Interfaces*, 2022, **14**, 23645–23652; (*f*) Y. Cheng, H. Wu, H. Yu, Z. Hu, J. Wang and Y. Wu, Rational Design of a Promising Oxychalcogenide Infrared Nonlinear Optical Crystal, *Chem. Sci.*, 2022, **13**, 5305–5310; (*g*) M.-Y. Ran, S.-H. Zhou, W. Wei, B. Li, X.-T. Wu, H. Lin and Q.-L. Zhu, Rational Design of a Rare-Earth Oxychalcogenide $Nd_3[Ga_3O_3S_3][Ge_2O_7]$ with Superior Infrared Nonlinear Optical Performance, *Small*, 2023, **19**, 2300248.

12 (*a*) M. Luo, K. Bu, Y. Liu, R. Wang, X. Zhang, C. Zheng, Q. Jin, X. Zhang and F. Huang, Synthesis, crystal structure, and optical properties of Ba_2SbO_2SX (X = Br, I) oxy-chalcohalides, *J. Solid State Chem.*, 2019, **278**, 1–4; (*b*) R. Wang, K. Bu, X. Zhang, Y. Gu, Y. Xiao, Z. Zhan and F. Q. Huang, A Novel Two-Dimensional Oxysulfide $Sr_{3.5}Pb_{2.5}Sb_6O_5S_{10}$: Synthesis, Crystal Structure, and Photoelectric Properties, *J. Mater. Chem. C*, 2020, **8**, 11018–11021; (*c*) H.-J. Zhao, H.-D. Yang, P.-F. Liu and H. Lin, From *Cc* to $P6_3mc$: Structural Variation in $La_3S_2Cl_2[SbS_3]$ and $La_3OSCl_2[SbS_3]$ Induced by the Isovalent Anion Substitution, *Cryst. Growth Des.*, 2022, **22**, 1437–1444.

13 (*a*) I. D. Brown and D. Altermatt, Bond-valence parameters obtained from a systematic analysis of the inorganic crystal structure database, *Acta Crystallogr., Sect. B: Struct. Sci.*, 1985, **41**, 244–247; (*b*) N. E. Brese and M. Okeeffe, Bond-valence parameters for solids, *Acta Crystallogr., Sect. B: Struct. Sci.*, 1991, **47**, 192–197.

14 (*a*) R. Dronskowski and P. E. Blochl, Crystal Orbital Hamilton Populations (COHP). Energy-Resolved Visualization of Chemical Bonding in Solids Based on Density-Functional Calculations, *J. Phys. Chem.*, 1993, **97**, 8617–8624; (*b*) H. Lin, Y. Y. Li, M. Y. Li, Z. J. Ma, L. M. Wu, X. T. Wu and Q. L. Zhu, Centric-to-acentric structure transformation induced by a stereochemically active lone pair: a new insight for design of IR nonlinear optical materials, *J. Mater. Chem. C*, 2019, **7**, 4638–4643.

15 R. Wang, Y. Zhao, X. Zhang and F. Huang, Structural dimension modulation in a new oxysulfide system of $Ae_2Sb_2O_2S_3$ (Ae = Ca and Ba), *Inorg. Chem. Front.*, 2022, **9**, 3552–3558.

16 F. Emmerling, S. Zimper and C. Roehr, New Barium Oxoantimonates(III): Synthesis and Crystal Structures of $Ba_3[SbO_3]_2$ and $Ba_2[Sb_2O_5]$, *Z. Naturforsch., B: J. Chem. Sci.*, 2004, **59**, 503–512.

17 (*a*) W. W. So, A. LaCour, V. O. Aliev and P. K. Dorhout, Synthesis and characterization of a new quaternary lanthanum oxythioantimonite: $La_6Sb_4O_{12}S_3$, *J. Alloys Compd.*, 2004, **374**, 234–239; (*b*) J. R. Panella, J. Chamorro and T. M. McQueen, Synthesis and Structure of Three New Oxychalcogenides: $A_2O_2Bi_2Se_3$ (A = Sr, Ba) and $Sr_2O_2Sb_2Se_3$, *Chem. Mater.*, 2016, **28**, 890–895; (*c*) R. Wang, F. Wang, X. Zhang, X. Feng, C. Zhao, K. Bu, Z. Zhang, T. Zhai and F. Q. Huang, Improved Polarization in the $Sr_6Cd_2Sb_6O_7Se_{10}$ Oxyselenide through Design of Lateral Sublattices for Efficient Photoelectric Conversion, *Angew. Chem., Int. Ed.*, 2022, **61**, e202206816; (*d*) R. Wang, F. Liang, F. Wang, Y. Guo, X. Zhang, Y. Xiao, K. Bu, Z. Lin, J. Yao, T. Zhai and F. Q. Huang, $Sr_6Cd_2Sb_6O_7S_{10}$: Strong SHG Response Activated by Highly Polarizable Sb/O/S Groups, *Angew. Chem., Int. Ed.*, 2019, **58**, 8078–8081; (*e*) D. Topa, J. Sejkora, E. Makovicky, J. Prsek, D. Ozdin, H. Putz, H. Dittrich and S. Karup-Moller, $Pb_{15-2x}Sb_{14+2x}S_{36}O_x$ (x similar to 0.2), a new sulphosalt species from the Low Tatra Mountains, Western Carpathians, Slovakia, *Eur. J. Mineral.*, 2012, **24**, 727–740; (*f*) Y. Moelo, A. Meerschaut, P. Orlandi and P. Palvadeau, Lead-antimony sulfosalts from Tuscany (Italy): II-Crystal structure of scainiite, $Pb_{14}Sb_{30}S_{54}O_5$, an expanded monoclinic derivative of $Ba_{12}Bi_{24}S_{48}$ hexagonal sub-type (zinkenite group), *Eur. J. Mineral.*, 2000, **12**, 835–846; (*g*) M. Nagao, M. Tanaka, R. Matsumoto, H. Tanaka, S. Watauchi, Y. Takano and I. Tanaka, Growth and Structure of Ce(O,F) SbS_2 Single Crystals, *Cryst. Growth Des.*, 2016, **16**, 3037–3042; (*h*) K. Bu, M. Luo, R. Wang, X. Zhang, J. He, D. Wang, W. Zhao and F. Q. Huang, Enhanced Photoelectric $SrOCuSbS_2$ of a [SrO]-Intercalated $CuSbS_2$ Structure, *Inorg. Chem.*, 2019, **58**, 69–72; (*i*) K. Bu, J. Huang, M. Luo, M. Guan, C. Zheng, J. Pan, X. Zhang, S. Wang, W. Zhao, X. Shi, L. Xu and F. Q. Huang, Observation of High Seebeck Coefficient and Low Thermal Conductivity in New [SrO]-intercalated $CuSbSe_2$ Compound, *Chem. Mater.*, 2018, **30**, 5539–5543; (*j*) Y. Wang, M. Luo, P. Zhao, X. Che, Y. Cao and F. Q. Huang, $Sr_4Pb_{1.5}Sb_5O_5Se_8$: a new mid-infrared nonlinear optical material with a moderate SHG response, *CrystEngComm*, 2020, **22**, 3526–3530; (*k*) I. Nakai, K. Koto, K. Nagashima and N. Morimoto, The crystal structure of sarabauite $CaSb_{10}O_{10}S_6$, a new oxide sulfide mineral, *Chem. Lett.*, 1977, **6**, 275–276.

18 (*a*) J. Androulakis, S. C. Peter, H. Li, C. D. Malliakas, J. A. Peters, Z. F. Liu, B. W. Wessels, J. H. Song, H. Jin, A. J. Freeman and M. G. Kanatzidis, Dimensional reduction: a design tool for new radiation detection materials, *Adv. Mater.*, 2011, **23**, 4163–4167; (*b*) H. Lin, L. H. Li and L. Chen, Diverse Closed Cavities in Condensed Rare Earth Metal–Chalcogenide Matrixes: Cs $[Lu_7Q_{11}]$ and $(ClCs_6)[RE_{21}Q_{34}]$ (RE = Dy, Ho; Q = S, Se, Te), *Inorg. Chem.*, 2012, **51**, 4588–4596; (*c*) H. Lin, J. N. Shen, Y. F. Shi, L. H. Li and L. Chen, Quaternary Rare-Earth Selenides with Closed Cavities: $Cs[RE_9Mn_4Se_{18}]$ (RE = Ho–Lu), *Inorg. Chem. Front.*, 2015, **2**, 298–305; (*d*) H. Chen, P. F. Liu, H. Lin, L. M. Wu and X. T. Wu, Solid-State Preparation, Structural Characterization, Physical Properties and Theoretical Studies of a Series of Novel Rare-earth Metal-Chalcogenides with Unprecedented Closed Cavities, *Cryst. Growth Des.*, 2019, **19**, 444–452.

19 (*a*) D. M. Yan, Y. Xiao, C. Liu, P. P. Hou, W. X. Chai, H. Hosono, H. Lin and Y. Liu, Two new members in the quaternary Cs-Ag-As-S family with different arrangements of Ag–S and As–S asymmetric building units: syntheses, structures, and theoretical studies, *Dalton Trans.*, 2020, **49**, 9743–9750; (*b*) C. Liu, H. D. Yang, P. P. Hou, Y. Xiao, Y. Liu and H. Lin, $Cs_3CuAs_4Q_8$ (Q = S, Se): unique two-dimensional layered inorganic thioarsenates with the lowest Cu-to-As ratio and remarkable photocurrent responses, *Dalton Trans.*, 2022, **51**, 904–909.

20 (*a*) S. N. Guin, A. Chatterjee, D. S. Negi, R. Datta and K. Biswas, High thermoelectric performance in tellurium free p-type $AgSbSe_2$, *Energy Environ. Sci.*, 2013, **6**, 2603–2608; (*b*) L.-D. Zhao, J. He, D. Berardan, Y. Lin, J.-F. Li, C.-W. Nan and N. Dragoe, BiCuSeO oxyselenides: new promising thermoelectric materials, *Energy Environ. Sci.*, 2014, **7**, 2900–2924; (*c*) G. J. Tan, L. D. Zhao and M. G. Kanatzidis, Rationally Designing High-Performance Bulk Thermoelectric Materials, *Chem. Rev.*, 2016, **116**, 12123–12149; (*d*) E. Nshimyimana, S. Hao, X. Su, C. Zhang, W. Liu, Y. Yan, C. Uher, C. Wolverton, M. G. Kanatzidis and X. Tang, Discordant nature of Cd in GeTe enhances phonon scattering and improves band convergence for high thermoelectric performance, *J. Mater. Chem. A*, 2020, **8**, 1193–1204; (*e*) L. Xie, D. He and J. He, SnSe, the rising star thermoelectric material: a new paradigm in atomic blocks, building intriguing physical properties, *Mater. Horiz.*, 2021, **8**, 1847–1865; (*f*) E. J. Blancas, J. J. Plata, J. Santana, F. Lemus-Prieto, A. M. Márquez and J. F. Sanz, Unraveling the role of chemical composition in the lattice thermal conductivity of oxychalcogenides as thermoelectric materials, *J. Mater. Chem. A*, 2022, **10**, 19941–19952.

21 (*a*) H. J. Goldsmid, in *CRC Handbook of Thermoelectrics*, ed. D. M. Rowe, CRC Press, Boca Raton, FL, 1995, p. 74; (*b*) H. Lin, H. Chen, J. N. Shen, L. Chen and L. M. Wu, Chemical Modification and Energetically Favorable Atomic Disorder of a Layered Thermoelectric Material $TmCuTe_2$ Leading to High Performance, *Chem. – Eur. J.*, 2014, **20**, 15401–15408; (*c*) H. Lin, H. Chen, N. Ma, Y. J. Zheng, J. N. Shen, J. S. Yu, X. T. Wu and L. M. Wu, Syntheses, Structures, and Thermoelectric Properties of Ternary Tellurides: $RECuTe_2$ (RE = Tb–Er), *Inorg. Chem. Front.*, 2017, **4**, 1273–1280.

22 (*a*) H. Lin, H. Chen, Y. J. Zheng, J. S. Yu and L. M. Wu, $AX_4^{II}X_5^{III}Te_{12}$ (A = Rb, Cs; X^{II} = Mn, Zn, Cd; X^{III} = Ga, In): quaternary semiconducting tellurides with very low thermal conductivities, *Dalton Trans.*, 2016, **45**, 17606–17609; (*b*) H. Chen, P.-F. Liu, H. Lin and X.-T. Wu, Ultralow thermal conductivity in the quaternary semiconducting chalcogenide $Cs_4[Ho_{26}Cd_7Se_{48}]$ with an unprecedented closed cavity architecture, *Inorg. Chem. Front.*, 2021, **8**, 1049–1055.

23 D. G. Cahill, S. K. Watson and R. O. Pohl, Lower limit to the thermal conductivity of disordered crystals, *Phys. Rev. B: Condens. Matter Mater. Phys.*, 1992, **46**, 6131–6140.

24 (*a*) H. Lin, H. Chen, Y. J. Zheng, Y. K. Chen, J. S. Yu and L. M. Wu, $Ba_5Cu_8In_2S_{12}$: a quaternary semiconductor with unique 3D copper-rich framework and ultralow thermal conductivity, *Chem. Commun.*, 2017, **53**, 2590–2593; (*b*) S. Jana, G. Panigrahi, M. Ishtiyak, S. Narayanswamy, P. P. Bhattacharjee, M. K. Niranjan and J. Prakash, Germanium Antimony Bonding in $Ba_4Ge_2Sb_2Te_{10}$ with Low Thermal Conductivity, *Inorg. Chem.*, 2021, **61**, 968–981; (*c*) W. Guo, Q. Huang, W.-L. Zhang, D.-G. Chen, A. Chen, E. H. Ang, H.-H. Cui, Z.-Z. Luo and Z. Zou, Two Mixed-Anion Semiconductors in the Ba–Sn–Te–S System with Low Thermal Conductivity, *ACS Appl. Energy Mater.*, 2023, **6**, 2508–2514.

25 (*a*) H. Lin, G. J. Tan, J. N. Shen, S. Q. Hao, L. M. Wu, N. Calta, C. Malliakas, S. Wang, C. Uher, C. Wolverton and M. G. Kanatzidis, Concerted Rattling in $CsAg_5Te_3$ Leading to Ultralow Thermal Conductivity and High Thermoelectric Performance, *Angew. Chem., Int. Ed.*, 2016, **55**, 11431–11436; (*b*) H. Chen, P.-F. Liu, H. Lin and X.-T. Wu, A new type of novel salt-inclusion chalcogenides with ultralow thermal conductivity, *Chem. Commun.*, 2020, **56**, 15149–15152; (*c*) P. Jafarzadeh, M. R. Rodrigues, Y. Shi, A. Assoud, T. Zou, J. B. Kycia and H. Kleinke, Effect of Mixed Occupancies on The Thermoelectric Properties of $BaCu_{6-x}Se_{1-y}Te_{6+y}$ Polychalcogenides, *Dalton Trans.*, 2019, **48**, 9357–9364.

26 L. You, Y. Liu, X. Li, P. Nan, B. Ge, Y. Jiang, P. Luo, S. Pan, Y. Pei, W. Zhang, G. J. Snyder, J. Yang, J. Zhang and J. Luo, Boosting the thermoelectric performance of PbSe through dynamic doping and hierarchical phonon scattering, *Energy Environ. Sci.*, 2018, **11**, 1848–1858.

27 H. Xie, X. Su, X. Zhang, S. Hao, T. P. Bailey, C. C. Stoumpos, A. P. Douvalis, X. Hu, C. Wolverton, V. P. Dravid, C. Uher, X. Tang and M. G. Kanatzidis, Origin of intrinsically low thermal conductivity in talnakhite $Cu_{17.6}Fe_{17.6}S_{32}$ thermoelectric material: correlations between lattice dynamics and thermal transport, *J. Am. Chem. Soc.*, 2019, **141**, 10905–10914.

28 R. Liu, L. Xi, H. Liu, X. Shi, W. Zhang and L. Chen, Ternary compound $CuInTe_2$: a promising thermoelectric material with diamond-like structure, *Chem. Commun.*, 2012, **48**, 3818–3820.

29 H. Xie, H. Wang, Y. Pei, C. Fu, X. Liu, G. J. Snyder, X. Zhao and T. Zhu, Beneficial Contribution of Alloy Disorder to Electron and Phonon Transport in Half-Heusler Thermoelectric Materials, *Adv. Funct. Mater.*, 2013, **23**, 5123–5130.

30 C. Fu, S. Bai, Y. Liu, Y. Tang, L. Chen, X. Zhao and T. Zhu, Realizing high figure of merit in heavy band p-type half-Heusler thermoelectric materials, *Nat. Commun.*, 2015, **6**, 8144.

31 Y. Qiu, L. Xi, X. Shi, P. Qiu, W. Zhang, L. Chen, J. R. Salvador, J. Y. Cho, J. Yang, Y.-C. Chien, S.-W. Chen, Y. Tang and G. J. Snyder, Charge-Compensated Compound Defects in Ga-containing Thermoelectric Skutterudites, *Adv. Funct. Mater.*, 2013, **23**, 3194–3203.

32 L. Fu, M. Yin, D. Wu, W. Li, D. Feng, L. Huang and J. He, Large enhancement of thermoelectric properties in n-type PbTe via dual-site point defects, *Energy Environ. Sci.*, 2017, **10**, 2030–2040.

33 G. Tan, L. D. Zhao, F. Shi, J. W. Doak, S. H. Lo, H. Sun, C. Wolverton, V. P. Dravid, C. Uher and M. G. Kanatzidis, High thermoelectric performance of p-type SnTe via a synergistic band engineering and nanostructuring approach, *J. Am. Chem. Soc.*, 2014, **136**, 7006–7017.

34 Y. Zheng, Q. Zhang, X. Su, H. Xie, S. Shu, T. Chen, G. Tan, Y. Yan, X. Tang, C. Uher and G. J. Snyder, Mechanically Robust BiSbTe Alloys with Superior Thermoelectric Performance: A Case Study of Stable Hierarchical Nanostructured Thermoelectric Materials, *Adv. Energy Mater.*, 2015, **5**, 1401391.

35 F. Li, J.-F. Li, L.-D. Zhao, K. Xiang, Y. Liu, B.-P. Zhang, Y.-H. Lin, C.-W. Nan and H.-M. Zhu, Polycrystalline BiCuSeO oxide as a potential thermoelectric material, *Energy Environ. Sci.*, 2012, **5**, 7188–7195.

36 L. D. Zhao, S. H. Lo, Y. S. Zhang, H. Sun, G. J. Tan, C. Uher, C. Wolverton, V. P. Dravid and M. G. Kanatzidis, Ultralow thermal conductivity and high thermoelectric figure of merit in SnSe crystals, *Nature*, 2014, **508**, 373–377.

37 (*a*) K. Burke, Perspective on density functional theory, *J. Chem. Phys.*, 2012, **136**, 150901; (*b*) Y.-F. Shi, S.-H. Zhou, B.-X. Li, Y. Liu, X.-T. Wu, H. Lin and Q.-L. Zhu, $Ba_5Ga_2SiO_4S_6$: a Phase-Matching Nonlinear Optical Oxychalcogenide Design via Structural Regulation Originated from Heteroanion Introduction, *Inorg. Chem.*, 2023, **62**, 464–473; (*c*) H. Chen, M.-Y. Ran, S.-H. Zhou, X.-T. Wu, H. Lin and Q.-L. Zhu, Simple yet extraordinary: super-polyhedra-built 3D chalcogenide framework of $Cs_5Ga_9S_{16}$ with excellent infrared nonlinear optical performance, *Chin. Chem. Lett.*, 2023, **34**, 107838.

38 (*a*) M. Y. Li, Y. X. Zhang, H. Lin, Z. J. Ma, X. T. Wu and Q. L. Zhu, Combined experimental and theoretical investigations of Ba_3GaS_4I: interesting structure transformation originated from the halogen substitution, *Dalton Trans.*, 2019, **48**, 17588–17593; (*b*) M.-Y. Ran, Z. Ma, X.-T. Wu, H. Lin and Q.-L. Zhu, $Ba_2Ge_2Te_5$: a ternary NLO-active telluride with unusual one-dimensional helical chains and giant second-harmonic-generation tensors, *Inorg. Chem. Front.*, 2021, **8**, 4838–4845; (*c*) Y. F. Shi, Z. Ma, B. X. Li, X. T. Wu, H. Lin and Q. L. Zhu, Phase matching achieved by isomorphous substitution in IR nonlinear optical material $Ba_2SnSSi_2O_7$ with an undiscovered $[SnO_4S]$ functional motif, *Mater. Chem. Front.*, 2022, **6**, 3054–3061; (*d*) H. D. Yang, S. H. Zhou, M. Y. Ran, X. T. Wu, H. Lin and Q. L. Zhu, Oxychalcogenides as Promising Ultraviolet Nonlinear Optical Candidates: Experimental and Theoretical Studies of $AEGeOS_2$ (AE = Sr and Ba), *Inorg. Chem.*, 2022, **61**, 15711–15720; (*e*) C. Zhang, S. H. Zhou, Y. Xiao, H. Lin and Y. Liu, Interesting dimensional transition through changing cations as the trigger in multinary thioarsenates displaying variable photocurrent response and optical anisotropy, *Inorg. Chem. Front.*, 2022, **9**, 5820–5827.

39 M. M. Chen, S. H. Zhou, W. B. Wei, B. X. Li, M. Y. Ran, X. T. Wu, H. Lin and Q. L. Zhu, $RbBiP_2S_6$: A Promising IR Nonlinear Optical Material with a Giant Second-Harmonic Generation Response Designed by Aliovalent Substitution, *ACS Mater. Lett.*, 2022, **4**, 1264–1269.

40 C. Liu, S.-H. Zhou, Y. Xiao, C. Zhang, H. Lin and Y. Liu, Aliovalent-cation-substitution-induced structure transformation: a new path toward high-performance IR nonlinear optical materials, *J. Mater. Chem. C*, 2021, **9**, 15407–15414.

41 C. Zhang, M. Y. Ran, X. Chen, S. H. Zhou, H. Lin and Y. Liu, Stereochemically active lone-pair-driven giant enhancement of birefringence from three-dimensional $CsZn_4Ga_5Se_{12}$ to two-dimensional $CsZnAsSe_3$, *Inorg. Chem. Front.*, 2023, **10**, 3367–3374.

42 C. Liu, S. H. Zhou, C. Zhang, Y. Y. Shen, X. Y. Liu, H. Lin and Y. Liu, $CsCu_3SbS_4$: rational design of a two-dimensional layered material with giant birefringence derived from Cu_3SbS_4, *Inorg. Chem. Front.*, 2022, **9**, 478–484.

